 CMES, vol.47, no.1, pp.61-95, 2009

Two- and Three-Dimensional Transient Thermoelastic Analysis by the MLPG Method

J. Sladek[1], V. Sladek[1], P. Solek[2], C.L. Tan[3] and Ch. Zhang[4]

Abstract: The meshless local Petrov-Galerkin (MLPG) method for transient linear thermoelastic analysis is presented. Orthotropic material properties are considered here. In uncoupled thermoelasticity, the temperature field is not influenced by displacements. Therefore, in the first step, the heat conduction equation is solved for the temperature distribution in the domain. The equations of motion are then solved with the inertial term considered. A Heaviside step function as the test functions is applied in the weak-form to derive local integral equations for solving two- and three-dimensional problems. Local integral equations are written on small sub-domains with circular or spherical shapes. They surround nodal points which are distributed over the analyzed domain. The spatial variation of the displacements and temperature are approximated by the moving least-squares (MLS) scheme. After performing the spatial integrations, a system of ordinary differential equations for certain nodal unknowns is obtained. The backward finite difference method is applied for the approximation of the diffusive term in the heat conduction equation. Then, the system of the ordinary differential equations of the second order resulting from the equations of motion is solved by the Houbolt finite-difference scheme as a time stepping method.

Keywords: Transient thermoelasticity, orthotropic materials, moving least-squares interpolation, Houbolt finite-difference scheme, crack problems, functionally graded materials

1 Indroduction

In recent years, meshless methods have become very popular computational tools for many engineering problems. This is due to their high adaptivity and low costs

[1] Institute of Construction and Architecture, Slovak Academy of Sciences, 84503 Bratislava, Slovakia
[2] Department of Mechanics, Slovak Technical University, Bratislava, Slovakia
[3] Department of Mechanical & Aerospace Engineering, Carleton University, Ottawa, Canada
[4] Department of Civil Engineering, University of Siegen, D-57068 Siegen, Germany

to prepare input and output data for numerical analyses. The moving least-squares (MLS) approximation is generally considered as one of many schemes to interpolate discrete data with a reasonable accuracy [Belytschko et al. (1996); Atluri and Shen (2002); Atluri (2004)]. The order of continuity of the MLS approximation is given by the minimum between the orders of continuity of the basis functions and that of the weight function. This allows the order of continuity to be tuned to a desired value. In conventional discretization methods, such as the finite element method (FEM) or the boundary element method (BEM), the interpolation functions usually result in a discontinuity of secondary fields (gradients of primary fields) on the interfaces of elements. For modeling continuously non-homogeneous solids, the approach based on piecewise continuous elements can yield some inaccuracies. Therefore, modeling based on C^1-continuity, such as in meshless methods, is expected to be more accurate than conventional discretization techniques. The meshless or generalized FEM methods are also very convenient for modeling cracks. One can embed particular enrichment functions at the crack-tip which enable the stress intensity factors to be compurted accurately [Fleming et al, (1997)].

The meshless method can be obtained from a weak-form formulation on either the global domain or a set of local subdomains. In the global formulation, background cells are required for the integration of the weak-form. In methods based on local weak-form formulation [Zhu et al. (1998), Atluri and Zhu (1998)], no background cells are required and therefore they are often referred to as truly meshless methods. The meshless local Petrov-Galerkin (MLPG) method is a fundamental base for the derivation of many meshless formulations since the trial and test functions can be chosen from different functional spaces. By using the fundamental solution as the test function, accurate numerical results can be obtained; this has been reported in previous papers for 2-D transient heat conduction problems in isotropic, homogeneous or continuously non-homogeneous solids [Sladek et al. (2003a,b), (2005a)] and elasticity problems under static and dynamic loads [Atluri et al. (2000, 2003); Sellountos and Polyzos (2003); Sellountos et al. (2005, 2009)]. Recently, the MLPG method with a Heaviside step function as the test functions [Atluri and Shen (2002), Atluri et al. (2003)] has been applied to solve two-dimensional homogeneous and continuously non-homogeneous elastic solids [Sladek et al., (2004b; 2009), (2008d)] and for 3-D problems in homogeneous and isotropic solids under a static or a dynamic load [Han and Atluri (2004a,b), Sladek et al. (2009)]. The present authors have recently analyzed 3-D axisymmetric dynamic problems in continuously non-homogeneous elastic solids [Sladek et al. (2005b), (2008e)] and heat conduction problems [Sladek et al. (2007a)]. The MLPG has also been successfully applied to 2-D piezoelectric problems [Sladek et al. (2007b)], 2-D and general 3-D heat conduction [Sladek et al. (2004a; 2008c)], plate and shell

problems [Sladek et al. (2008a,b)].

In recent years, the application of composite materials has increased in many areas of technology. Composites consist of two or more materials mixed in various manners. If volume fractions of the constituents vary gradually in space in a pre-determined profile, such solids are referred to as functionally graded materials (FGMs). FGMs possess some advantages over conventional composites because of their continuously graded composition and properties [Suresh and Mortensen (1998); Miyamoto et al. (1999)]. FGMs may exhibit isotropic or anisotropic material properties, depending on the processing technique and the practical engineering requirements. Recent progress in the development and research of FGMs has also enhanced interests in the development of numerical methods for the solution of elastic and thermoelastic problems in continuously non-homogeneous solids. One can find in the literature works concerning mainly elastic or heat conduction problems in FGMs with exponential variations of material properties and under steady-state boundary conditions [Noda and Jin (1993); Erdogan and Wu (1996); Jin and Noda (1993)]. Transient heat transfer in FGMs with the exponential spatial variation has also been examined, but to a lesser extent [Jin and Batra, 1996; Noda and Jin (1994); Jin and Paulino (2001); Sutradhar et al. (2002); Jin (2002)]. The first numerical studies of elastic FGMs have been carried out using the finite element method [Santare and Lambros (2000); Anlas et al. (2000); Kim and Paulino (2002)]. The boundary element method (BEM) is a very powerful computational method if the fundamental solution is available. Anisotropy increases the number of elastic constants in Hooke's law, hence the construction of fundamental solutions becomes difficult even in a homogeneous medium. The fundamental solution is available in closed form for 2-D problems in a homogeneous, anisotropic, linear elastic solid [Eshelby et al. (1953); Schclar (1994)] and it is given in a complex variable space. Recently, Shiah et al. (2008) have presented an explicit form of the fundamental solutions for displacements and stresses in 3-D anisotropic elastic solids. Governing equations for continuously non-homogeneous solids are more complicated than for their homogeneous counterparts. To the present authors' knowledge, the fundamental solutions for general functionally graded materials are not available in 2-D and 3-D elasticity. However, those for problems in exponentially graded, isotropic, linear elastic materials have been derived recently [Martin et al. (2002); Chan et al. (2004); Criado et al. (2008).

Dynamic thermoelasticity is relevant for many engineering problems since thermal stresses play an important role in the integrity of structures. Several computational methods have been proposed over the past years to analyze thermoelasticity problems in homogeneous or piece-wise homogeneous materials. Shiah and Tan (1999) applied the BEM for 2-D uncoupled thermoelasticity in anisotropic solids.

Particular integral formulations for 2-D and 3-D transient uncoupled thermoelastic analyses have been presented by Park and Banerjee (2002). The BEM has been successfully applied also to coupled thermoelastic problems [Sladek and Sladek (1984); Dargush and Banerjee (1991); Chen and Dargush (1995); Suh and Tosaka (1989); Hosseini-Tehrani and Eslami (2000); Keppas et al. (2008)]. Dual reciprocity BEM has been presented by Gaul *et al.* (2003), and Kögl and Gaul (2003). A variety of meshless methods has been proposed so far and some of them also applied to transient heat conduction problems [Batra et al. (2004); Sladek et al. (2003a,b, 2004a, 2005a); Wang et al. (2006)] or to thermoelastic problems [Sladek et al. (2001, 2006); Bobaru and Mukherjee (2003); Qian and Batra (2004); Ching and Chen (2006)]. The present authors are not aware of any paper in the literature devoted to a meshless treatment of 2-D and 3-D thermoelastic problems in FGM with anisotropic material properties.

In this paper, the MLPG method is applied to solving two- and three-dimensional transient uncoupled thermoelasticity problems. Orthotropic material properties are considered here. In uncoupled thermoelasticity, the temperature field is not influenced by displacements. Therefore, the heat conduction equation is solved first to obtain the temperature distribution. The equation of motion is subsequently solved with the inertial term. In the process, nodal points are introduced and distributed over the analyzed domain, each of which is surrounded by a small circle for 2-D and a small sphere for 3-D problems. The weak-form on small subdomains with a Heaviside step function as the test functions is applied to derive local integral equations. The spatial variation of the displacements and temperature are approximated by the moving least-squares (MLS) scheme. After performing the spatial integrations, a system of ordinary differential equations for certain nodal unknowns is obtained. The backward finite difference method is applied for the approximation of the diffusive term in the heat conduction equation. Then, the system of the ordinary differential equations of the second order resulting from the equations of motion is solved by the Houbolt finite-difference scheme as a time stepping method.

2 The MLPG in transient uncoupled thermoelasticity

Consider a continuously non-homogeneous, orthotropic, linear elastic solid. The equilibrium and the thermal balance equations in transient uncoupled thermoelasticity [Nowacki (1986)] can be written as

$$\sigma_{ij,j}(\mathbf{x},\tau) - \rho \ddot{u}_i(\mathbf{x},\tau) + X_i(\mathbf{x},\tau) = 0, \tag{1}$$

$$[k_{ij}(\mathbf{x})\theta_{,j}(\mathbf{x},\tau)]_{,i} - \rho c \dot{\theta}(\mathbf{x},\tau) + Q(\mathbf{x},\tau) = 0, \tag{2}$$

where σ_{ij}, θ, u_i, X_i and Q are the stresses, temperature difference, displacements, density of body force vector and density of heat sources, respectively. Also, ρ,

$k_{ij}$and c are the mass density, thermal conductivity tensor and specific heat, respectively. The dots over a quantity indicate the derivatives with respect to time. A static problem can be considered formally as a special case of the dynamic one, by omitting the acceleration $\ddot{u}_i(\mathbf{x},\tau)$ in the equations of motion (1) and the time derivative term in equation (2). Therefore, both cases are analyzed in this paper simultaneously.

In the case of orthotropic materials, the relation between the stresses σ_{ij} and the strains ε_{ij} including the thermal expansion, is given by the well known Duhamel-Neumann constitutive equations for the stress tensor

$$\sigma_{ij}(\mathbf{x},\tau) = c_{ijkl}\varepsilon_{kl}(\mathbf{x},\tau) - \gamma_{ij}\theta(\mathbf{x},\tau), \tag{3}$$

where $c_{ijkl}$are the materials elastic coefficients and $\gamma_{ij}$is the stress-temperature modulus. The stress-temperature modulus can be expressed through the elastic coefficients and the coefficients of linear thermal expansion α_{kl}as

$$\gamma_{ij} = c_{ijkl}\alpha_{kl}. \tag{4}$$

For 2-D plane problems, the constitutive equation (3) is frequently written in terms of the second-order tensor of elastic constants [Lekhnitskii (1963)]. The constitutive equation for orthotropic materials and plane strain problems has the following form

$$\begin{bmatrix}\sigma_{11}\\ \sigma_{22}\\ \sigma_{12}\end{bmatrix} = \begin{bmatrix}c_{11} & c_{12} & 0\\ c_{12} & c_{22} & 0\\ 0 & 0 & c_{66}\end{bmatrix}\begin{bmatrix}\varepsilon_{11}\\ \varepsilon_{22}\\ 2\varepsilon_{12}\end{bmatrix} - \begin{bmatrix}c_{11} & c_{12} & c_{13}\\ c_{12} & c_{22} & c_{23}\\ 0 & 0 & 0\end{bmatrix}\begin{bmatrix}\alpha_{11}\\ \alpha_{22}\\ \alpha_{33}\end{bmatrix}\theta = \mathbf{C}\begin{bmatrix}\varepsilon_{11}\\ \varepsilon_{22}\\ 2\varepsilon_{12}\end{bmatrix} - \boldsymbol{\gamma}\theta, \tag{5}$$

with

$$\boldsymbol{\gamma} = \begin{bmatrix}c_{11} & c_{12} & c_{13}\\ c_{12} & c_{22} & c_{23}\\ 0 & 0 & 0\end{bmatrix}\begin{bmatrix}\alpha_{11}\\ \alpha_{22}\\ \alpha_{33}\end{bmatrix} = \begin{bmatrix}\gamma_{11}\\ \gamma_{22}\\ 0\end{bmatrix}.$$

Equation (5) can be reduced to a simple form for isotropic materials

$$\sigma_{ij} = 2\mu\varepsilon_{ij} + \lambda\varepsilon_{kk}\delta_{ij} - (3\lambda + 2\mu)\alpha\theta\delta_{ij}, \tag{6}$$

with Lame's constants λ and μ.

The constitutive equations for 3-D problems in orthotropic materials can be written as

$$\begin{bmatrix}\sigma_{11}\\ \sigma_{22}\\ \sigma_{33}\\ \sigma_{23}\\ \sigma_{13}\\ \sigma_{12}\end{bmatrix} = \begin{bmatrix} c_{11} & c_{12} & c_{13} & 0 & 0 & 0\\ c_{12} & c_{22} & c_{23} & 0 & 0 & 0\\ c_{13} & c_{23} & c_{33} & 0 & 0 & 0\\ 0 & 0 & 0 & c_{44} & 0 & 0\\ 0 & 0 & 0 & 0 & c_{55} & 0\\ 0 & 0 & 0 & 0 & 0 & c_{66}\end{bmatrix} \begin{bmatrix}\varepsilon_{11}\\ \varepsilon_{22}\\ \varepsilon_{33}\\ 2\varepsilon_{23}\\ 2\varepsilon_{13}\\ 2\varepsilon_{12}\end{bmatrix} - \begin{bmatrix} c_{11} & c_{12} & c_{13}\\ c_{12} & c_{22} & c_{23}\\ c_{13} & c_{23} & c_{33}\\ 0 & 0 & 0\\ 0 & 0 & 0\\ 0 & 0 & 0\end{bmatrix} \begin{bmatrix}\alpha_{11}\\ \alpha_{22}\\ \alpha_{33}\end{bmatrix} \theta$$

$$= \mathbf{C} \begin{bmatrix}\varepsilon_{11}\\ \varepsilon_{22}\\ \varepsilon_{33}\\ 2\varepsilon_{23}\\ 2\varepsilon_{13}\\ 2\varepsilon_{12}\end{bmatrix} - \boldsymbol{\gamma}\theta. \tag{7}$$

The compliance coefficients β_{ij} are obtained by the inversion of the matrix $\mathbf{C}$. For orthotropic materials they can be expressed in terms of engineering constants, namely, the Young's moduli and Poisson's ratios, as

$$\beta_{11} = 1/E_1, \quad \beta_{22} = 1/E_2, \quad \beta_{33} = 1/E_3,$$

$$\beta_{12} = \beta_{21} = -\nu_{12}/E_1 = -\nu_{21}/E_2, \quad \beta_{13} = \beta_{31} = -\nu_{13}/E_1 = -\nu_{31}/E_3,$$

$$\beta_{23} = \beta_{32} = -\nu_{23}/E_2 = -\nu_{32}/E_3, \quad \beta_{44} = 1/G_{23},$$

$$\beta_{55} = 1/G_{13}, \quad \beta_{66} = 1/G_{12}, \tag{8}$$

where E_k is the Young's modulus with respect to the $x_k$axis, $G_{12}$is the shear modulus for the $x_1 - x_2$ plane and ν_{ij} are Poisson's ratios.

The following essential and natural boundary conditions are assumed for the mechanical quantities

$$u_i(\mathbf{x},\tau) = \tilde{u}_i(\mathbf{x},\tau) \text{ on } \Gamma_u,$$

$$t_i(\mathbf{x},\tau) = \sigma_{ij}(\mathbf{x},\tau)n_j(\mathbf{x}) = \tilde{t}_i(\mathbf{x},\tau) \text{ on } \Gamma_t,$$

and for the thermal quantities

$$\theta(\mathbf{x},\tau) = \tilde{\theta}(\mathbf{x},\tau) \text{ on } \Gamma_p,$$

$$q(\mathbf{x},\tau) = k_{ij}\theta_{,j}(\mathbf{x},\tau)n_i(\mathbf{x}) = \tilde{q}(\mathbf{x},\tau) \text{ on } \Gamma_q,$$

where Γ_u is the part of the global boundary with prescribed displacements, while on Γ_t, Γ_p and Γ_q the traction vector t_i, the temperature and the heat flux q are prescribed, respectively.

Initial conditions for the mechanical and thermal quantities are prescribed as

$$u_i(\mathbf{x},\tau)|_{\tau=0} = u_i(x,0) \text{ and } \dot{u}_i(\mathbf{x},\tau)|_{\tau=0} = \dot{u}_i(x,0)$$

$$\theta(\mathbf{x},\tau)|_{\tau=0} = \theta(x,0) \text{ in } \Omega.$$

The local weak-form of the governing equations (1) can be written as [Atluri, (2004), Sladek et al. (2009)]

$$\int_{\Omega_s} [\sigma_{ij,j}(\mathbf{x},\tau) - \rho\ddot{u}_i(\mathbf{x},\tau) + X_i(\mathbf{x},\tau)]\, u^*_{ik}(\mathbf{x}) d\Omega = 0, \tag{9}$$

where $u^*_{ik}(\mathbf{x})$ is a test function.

Applying the Gauss divergence theorem to the first integral results in

$$\int_{\partial\Omega_s} \sigma_{ij}(\mathbf{x},\tau) n_j(\mathbf{x}) u^*_{ik}(\mathbf{x}) d\Gamma - \int_{\Omega_s} \sigma_{ij}(\mathbf{x},\tau) u^*_{ik,j}(\mathbf{x}) d\Omega + \int_{\Omega_s} [-\rho\ddot{u}_i(\mathbf{x},\tau) + X_i(\mathbf{x},\tau)]\, u^*_{ik}(\mathbf{x}) d\Omega = 0, \tag{10}$$

where $\partial\Omega_s$ is the boundary of the local subdomain which consists of three parts $\partial\Omega_s = L_s \cup \Gamma_{st} \cup \Gamma_{su}$ in general [Atluri, (2004)] (Fig. 1). For simplicity the same symbols are used for 2-D and 3-D problems. Here, L_s is the local boundary that is totally inside the global domain, Γ_{st} is the part of the local boundary which coincides with the global traction boundary, i.e., $\Gamma_{st} = \partial\Omega_s \cap \Gamma_t$, and similarly Γ_{su} is the part of the local boundary that coincides with the global displacement boundary, i.e., $\Gamma_{su} = \partial\Omega_s \cap \Gamma_u$.

By choosing a Heaviside step function as the test function $u^*_{ik}(\mathbf{x})$ in each subdomain

$$u^*_{ik}(\mathbf{x}) = \begin{cases} \delta_{ik} & \text{at} \mathbf{x} \in \Omega_s \\ 0 & \text{at} \mathbf{x} \notin \Omega_s \end{cases},$$

the local weak-form (10) is converted into the following local boundary-domain integral equations

$$\int_{L_s+\Gamma_{su}} t_i(\mathbf{x},\tau) d\Gamma - \int_{\Omega_s} \rho\ddot{u}_i(\mathbf{x},\tau) d\Omega = -\int_{\Gamma_{st}} \tilde{t}_i(\mathbf{x},\tau) d\Gamma - \int_{\Omega_s} X_i(\mathbf{x},\tau) d\Omega. \tag{11}$$

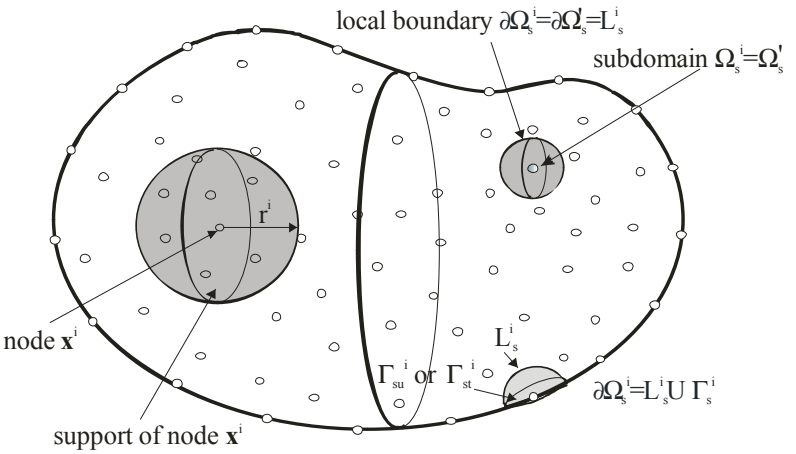

Figure 1: Local boundaries for weak-form formulation and support domain of weight function at node $\mathbf{x}^i$

Equation (11) is recognized as the overall momentum equilibrium conditions on the subdomain Ω_s. Note that the local integral equations (LIEs) (11) are valid for both homogeneous and non-homogeneous solids. Non-homogeneous material properties are included in eq. (11) through the elastic and thermo-elastic coefficients involved in the traction components

$$t_i(\mathbf{x},\tau) = \left[c_{ijkl}(\mathbf{x})u_{k,l}(\mathbf{x},\tau) - \lambda_{ij}(\mathbf{x})\theta(\mathbf{x},\tau)\right] n_j(\mathbf{x}).$$

Similarly, the local weak-form of the governing equation (2) can be written as

$$\int_{\Omega_s} \left\{ \left[k_{ij}(\mathbf{x})\theta_{,j}(\mathbf{x},\tau)\right]_{,i} - \rho c\dot{\theta}(\mathbf{x},\tau) + Q(\mathbf{x},\tau) \right\} u^*(\mathbf{x}) d\Omega = 0, \tag{12}$$

where $u^*(\mathbf{x})$ is a test function.

Applying the Gauss divergence theorem to the local weak-form and considering the Heaviside step function for the test function $u^*(\mathbf{x})$, one can obtain

$$\int_{L_s+\Gamma_{sp}} q(\mathbf{x},\tau)d\Gamma - \int_{\Omega_s} \rho c\dot{\theta}(x,\tau)d\Omega = -\int_{\Gamma_{sq}} \tilde{q}(\mathbf{x},\tau)d\Gamma - \int_{\Omega_s} Q(\mathbf{x},\tau)d\Omega. \tag{13}$$

Equation (13) is similarly recognized as the energy balance condition on the subdomain.

3 Numerical solution

In the MLPG method, the test and trial functions are not necessarily from the same functional spaces. For internal nodes, the test function is chosen as the Heaviside step function with support on the local subdomain. The trial function, on the other hand, is chosen to be the moving least-squares (MLS) approximation over a number of nodes randomly spread within the domain of influence. While the local subdomain is defined as the support of the test function on which the integration is carried out, the domain of influence is defined as a region where the weight function is not zero and all nodes lying inside are considered for interpolation. To approximate the distribution of displacements over a number of randomly located nodes$\{x^a\}$, $a = 1,2,...,n$, the MLS approximant $u^h(\mathbf{x},\tau)$ of $\bar{u}$ is defined by

$$u^h(\mathbf{x},\tau) = \mathbf{p}^T(\mathbf{x})\mathbf{a}(\mathbf{x},\tau), \tag{14}$$

where $\mathbf{p}^T(\mathbf{x}) = \left[p^1(\mathbf{x}), p^2(\mathbf{x}), ..., p^m(\mathbf{x})\right]$ is a complete monomial basis of order m; and $\mathbf{a}(\mathbf{x})$ is a vector containing the coefficients $a^j(\mathbf{x})$, $j = 1,2,...,m$which are functions of the space co-ordinates $\mathbf{x} = [x_1, x_2, x_3]^T$. For example, in 2-D problems

$$\mathbf{p}^T(\mathbf{x}) = \{1, x_1, x_2\} \text{ for } m = 3$$

and

$$\mathbf{p}^T(\mathbf{x}) = \left\{1, x_1, x_2, x_1^2, x_1x_2, x_2^2\right\} \text{ for } m = 6 \tag{15}$$

are linear and quadratic basis functions, respectively.

In 3-D problems, the linear basis is defined as

$$\mathbf{p}^T(\mathbf{x}) = [1, x_1, x_2, x_3], \tag{16}$$

and the quadratic basis is defined as

$$\mathbf{p}^T(\mathbf{x}) = \left[1, x_1, x_2, x_3, x_1^2, x_2^2, x_3^2, x_1x_2, x_1x_3, x_3x_2\right]. \tag{17}$$

The coefficient vector$\mathbf{a}(\mathbf{x})$is determined by minimizing a weighted discreteL_2-norm defined as

$$J(\mathbf{x}) = \sum_{a=1}^{n} w^a(\mathbf{x}) \left[\mathbf{p}^T(\mathbf{x}^a)\mathbf{a}(\mathbf{x},\tau) - \hat{\mathbf{u}}^a(\tau)\right]^2, \tag{18}$$

where $w^a(\mathbf{x})$ is the weight function associated with the node a with $w^a(\mathbf{x}) \geq 0$. Recall that n is the number of nodes in the support domain for which the weight function $w^a(\mathbf{x}) > 0$ and $\hat{\mathbf{u}}^a(\tau)$ are the fictitious nodal values, but not the nodal values

of the unknown trial function $\bar{\mathbf{u}}^h(\mathbf{x},\tau)$in general. The stationary condition of Jin eq. (18) with respect to $\mathbf{a}(\mathbf{x},\tau)$,

$$\partial J/\partial \mathbf{a} = 0,$$

leads to the following linear relation between $\mathbf{a}(\mathbf{x},\tau)$ and $\hat{\mathbf{u}}(\tau)$

$$\mathbf{A}(\mathbf{x})\mathbf{a}(\mathbf{x},\tau) - \mathbf{B}(\mathbf{x})\hat{\mathbf{u}}(\tau) = 0, \tag{19}$$

where

$$\mathbf{A}(\mathbf{x}) = \sum_{a=1}^{n} w^a(\mathbf{x})\mathbf{p}(\mathbf{x}^a)\mathbf{p}^T(\mathbf{x}^a),$$

$$\mathbf{B}(\mathbf{x}) = \left[w^1(\mathbf{x})\mathbf{p}(\mathbf{x}^1), w^2(\mathbf{x})\mathbf{p}(\mathbf{x}^2), ..., w^n(\mathbf{x})\mathbf{p}(\mathbf{x}^n)\right]. \tag{20}$$

The MLS approximation is well defined only when the matrix $\mathbf{A}$ in eq. (20) is non-singular. A necessary condition to satisfy this requirement is that at least m weight functions are non-zero (i.e. $n \geq m$) for each sample point $\mathbf{x} \in \Omega$. The solution of eq. (19) for $\mathbf{a}(\mathbf{x},\tau)$ and a subsequent substitution into eq. (14) lead to the following relation

$$\mathbf{u}^h(\mathbf{x},\tau) = \mathbf{\Phi}^T(\mathbf{x}) \cdot \hat{\mathbf{u}}(\tau) = \sum_{a=1}^{n} \phi^a(\mathbf{x})\hat{\mathbf{u}}^a(\tau), \tag{21}$$

where

$$\mathbf{\Phi}^T(\mathbf{x}) = \mathbf{p}^T(\mathbf{x})\mathbf{A}^{-1}(\mathbf{x})\mathbf{B}(\mathbf{x}). \tag{22}$$

Similarly, the temperature field is approximated as

$$\theta^h(\mathbf{x},\tau) = \sum_{a=1}^{n} \phi^a(\mathbf{x})\hat{\theta}^a(\tau).$$

In eq. (21), $\phi^a(\mathbf{x})$ is usually referred to as the shape function of the MLS approximation corresponding to the nodal point $\mathbf{x}^a$. From eqs. (20) and (22), it can be seen that $\phi^a(\mathbf{x}) = 0$ when $w^a(\mathbf{x}) = 0$. In practical applications, $w^a(\mathbf{x})$ is often chosen such that it is non-zero over a finite support of the nodal point $\mathbf{x}_i$. The support of the nodal point $\mathbf{x}^a$ is usually taken to be a sphere of the radius r_i centered at $\mathbf{x}^a$ (see Fig. 1). The radius r_i is an important parameter of the MLS approximation because it determines the range of the interaction (coupling) between the degrees of freedom defined at the nodes considered.

A 4^{th}-order spline-type weight function is applied in the present work

$$w^a(\mathbf{x}) = \begin{cases} 1-6\left(\frac{d^a}{r^a}\right)^2+8\left(\frac{d^a}{r^a}\right)^3-3\left(\frac{d^a}{r^a}\right)^4 & 0 \le d^a \le r^a \\ 0 & d^a \ge r^a \end{cases}, \tag{23}$$

where $d^a = \|\mathbf{x}-\mathbf{x}^a\|$ and r^a is the radius of the circular (2-D) and spherical (3-D) support domain. With eq. (23), the C^1-continuity of the weight function is ensured over the entire domain; thus, the continuity condition of the traction vector and the heat flux is satisfied.

The partial derivatives of the MLS shape functions are obtained as [Atluri (2004)]

$$\phi^a_{,k} = \sum_{j=1}^{m}\left[p^j_{,k}(\mathbf{A}^{-1}\mathbf{B})^{ja} + p^j(\mathbf{A}^{-1}\mathbf{B}_{,k}+\mathbf{A}^{-1}_{,k}\mathbf{B})^{ja}\right], \tag{24}$$

wherein $\mathbf{A}^{-1}_{,k} = \left(\mathbf{A}^{-1}\right)_{,k}$ represents the derivative of the inverse of $\mathbf{A}$ with respect to x_k, which is given by

$$\mathbf{A}^{-1}_{,k} = -\mathbf{A}^{-1}\mathbf{A}_{,k}\mathbf{A}^{-1}.$$

The traction vectors $t_i(\mathbf{x},\tau)$ at a boundary point $\mathbf{x} \in \partial\Omega_s$ are approximated in terms of the same nodal values $\hat{\mathbf{u}}^a(\tau)$ and $\hat{\theta}^a(\tau)$ as

$$\mathbf{t}^h(\mathbf{x},\tau) = \mathbf{N}(\mathbf{x})\mathbf{C}\sum_{a=1}^{n}\mathbf{B}^a(\mathbf{x})\hat{\mathbf{u}}^a(\tau) - \mathbf{N}(\mathbf{x})\boldsymbol{\gamma}\sum_{a=1}^{n}\phi^a(\mathbf{x})\hat{\theta}^a(\tau), \tag{25}$$

where the matrix **N(x)** is related to the normal vector **n(x)** on $\partial\Omega_s$ by

$$\mathbf{N}(\mathbf{x}) = \begin{bmatrix} n_1 & 0 & 0 & 0 & n_3 & n_2 \\ 0 & n_2 & 0 & n_3 & 0 & n_1 \\ 0 & 0 & n_3 & n_2 & n_1 & 0 \end{bmatrix}$$

for 3-D, and

$$\mathbf{N}(\mathbf{x}) = \begin{bmatrix} n_1 & 0 & n_2 \\ 0 & n_2 & n_1 \end{bmatrix}$$

for 2-D problems.

The matrix $\mathbf{B}^a$ is represented by the gradients of the shape functions for 3-D as

$$\mathbf{B}^a = \begin{bmatrix} \phi^a_{,1} & 0 & 0 \\ 0 & \phi^a_{,2} & 0 \\ 0 & 0 & \phi^a_{,3} \\ 0 & \phi^a_{,3} & \phi^a_{,2} \\ \phi^a_{,3} & 0 & \phi^a_{,1} \\ \phi^a_{,2} & \phi^a_{,1} & 0 \end{bmatrix}$$

and

$$\mathbf{B}^a(\mathbf{x}) = \begin{bmatrix} \varphi^a_{,1} & 0 \\ 0 & \varphi^a_{,2} \\ \varphi^a_{,2} & \varphi^a_{,1} \end{bmatrix}$$

for 2-D problems.

Similarly the heat flux $q(\mathbf{x},\tau)$ can be approximated by

$$q^h(\mathbf{x},\tau) = k_{ij} n_i \sum_{a=1}^{n} \phi^a_{,j}(\mathbf{x}) \hat{\theta}^a(\tau). \tag{26}$$

The local integral equation for the heat conduction, eq. (13), at the source point $\mathbf{x}^i$ located inside Ω, yields the following set of equations

$$\sum_{a=1}^{n} \hat{\theta}^a(\tau) \int_{\partial\Omega_s^i} \mathbf{n}^T(\mathbf{x}) \mathbf{K}(\mathbf{x}) \mathbf{P}^a(\mathbf{x}) d\Gamma - \sum_{a=1}^{n} \dot{\hat{\theta}}^a(\tau) \int_{\Omega_s^i} \rho c \phi^a(\mathbf{x}) d\Omega = -\int_{\Omega_s^i} Q(\mathbf{x},\tau) d\Omega \tag{27}$$

where for 3-D problems

$$\mathbf{K}(\mathbf{x}) = \begin{bmatrix} k_{11} & k_{12} & k_{13} \\ k_{12} & k_{22} & k_{23} \\ k_{13} & k_{23} & k_{33} \end{bmatrix}, \quad \mathbf{P}^a(\mathbf{x}) = \begin{bmatrix} \phi^a_{,1} \\ \phi^a_{,2} \\ \phi^a_{,3} \end{bmatrix}, \quad \mathbf{n}^T = (n_1, n_2, n_3)$$

and for 2-D problems

$$\mathbf{K}(\mathbf{x}) = \begin{bmatrix} k_{11} & k_{12} \\ k_{12} & k_{22} \end{bmatrix}, \quad \mathbf{P}^a(\mathbf{x}) = \begin{bmatrix} \phi^a_{,1} \\ \phi^a_{,2} \end{bmatrix}, \quad \mathbf{n}^T = (n_1, n_2).$$

Substituting the MLS approximations for displacements (21) and tractions (25) into (11) for each of the internal nodes $\mathbf{x}^i$, the following set of discretized LIEs for mechanical fields is obtained

$$\sum_{a=1}^{n} \left[\left(\int_{L_s^i} \mathbf{N}(\mathbf{x}) \mathbf{C} \mathbf{B}^a(\mathbf{x}) d\Gamma \right) \hat{\mathbf{u}}^a(\tau) - \rho \left(\int_{\Omega_s^i} \phi^a(\mathbf{x}) d\Omega \right) \ddot{\hat{\mathbf{u}}}^a(\tau) \right] - \sum_{a=1}^{n} \left(\int_{L_s + \Gamma_{su}} \mathbf{N}(\mathbf{x}) \boldsymbol{\gamma} \phi^a(\mathbf{x}) d\Gamma \right) \hat{\theta}^a(\tau) = -\int_{\Omega_s^i} \mathbf{X}(\mathbf{x},\tau) d\Omega. \tag{28}$$

The discretized displacement, traction, temperature and heat flux boundary conditions

$$\sum_{a=1}^{n} \phi^a(\mathbf{x}^i)\hat{\mathbf{u}}^a(\tau) = \tilde{\mathbf{u}}(\mathbf{x}^i,\tau) \text{ for } \mathbf{x}^i \in \Gamma_{su}^i, \tag{29}$$

$$\mathbf{N}(\mathbf{x}^i)\mathbf{C}\sum_{a=1}^{n} \mathbf{B}^a(\mathbf{x}^i)\hat{\mathbf{u}}^a(\tau) - \mathbf{N}(\mathbf{x}^i)\boldsymbol{\gamma}\sum_{a=1}^{n} \phi^a(\mathbf{x}^i)\hat{\theta}^a(\tau) = \tilde{\mathbf{t}}(\mathbf{x}^i,\tau) \text{ for } \mathbf{x}^i \in \Gamma_{st}^i, \tag{30}$$

$$\sum_{a=1}^{n} \phi^a(\mathbf{x}^i)\hat{\theta}^a(\tau) = \tilde{\theta}(\mathbf{x}^i,\tau) \text{ for } \mathbf{x}^i \in \Gamma_{sp}, \tag{31}$$

$$\sum_{a=1}^{n} \mathbf{n}^T(\mathbf{x}^i)\mathbf{K}(\mathbf{x}^i)\mathbf{P}^a(\mathbf{x}^i)\hat{\theta}^a(\tau) = \tilde{q}(\mathbf{x}^i,\tau) \text{ for } \mathbf{x}^i \in \Gamma_{sq}^i \tag{32}$$

are considered at boundary nodes Γ_u, Γ_t, Γ_p and Γ_q, respectively.

The backward finite difference method is applied for the approximation of "velocities"

$$\dot{\mathbf{y}}_{\tau+\Delta\tau} = \frac{\mathbf{y}_{\tau+\Delta\tau} - \mathbf{y}_\tau}{\Delta\tau}, \tag{33}$$

where $\Delta\tau$ is the time step.

The system of ordinary differential equations (27) and collocation equations (31) and (32) can be rearranged in such a way that all known quantities are in the second member of the matrix form the system equations, viz.

$$\mathbf{A}\dot{\mathbf{y}} + \mathbf{B}\mathbf{y} = \mathbf{Q}. \tag{34}$$

Substituting eq. (33) into eq. (34) results in the following set of algebraic equations for the unknowns $\mathbf{y}_{\tau+\Delta\tau}$

$$\left[\frac{1}{\Delta\tau}\mathbf{A} + \mathbf{B}\right]\mathbf{y}_{\tau+\Delta\tau} = \mathbf{A}\frac{1}{\Delta\tau}\left\{\mathbf{y}_{\tau-\Delta\tau}\right\} + \mathbf{Q}. \tag{35}$$

Once the temperature field is computed from eq. (35), the mechanical fields can be determined. The matrix form of ordinary differential equations (28) and collocation equations (29) and (30) can be written as

$$\mathbf{L}\ddot{\mathbf{x}} + \mathbf{K}\mathbf{x} = \mathbf{P}. \tag{36}$$

Several time integration procedures for the solution of this system of ordinary differential equations are available. In the present work, the Houbolt finite difference

scheme [Houbolt (1950)] is adopted in which the acceleration $\ddot{\mathbf{u}} = \ddot{\mathbf{x}}$ is expressed as

$$\ddot{\mathbf{x}}_{\tau+\Delta\tau} = \frac{2\mathbf{x}_{\tau+\Delta\tau} - 5\mathbf{x}_{\tau} + 4\mathbf{x}_{\tau-\Delta\tau} - \mathbf{x}_{\tau-2\Delta\tau}}{\Delta\tau^2}, \tag{37}$$

where $\Delta\tau$ is the time step.

Substituting eq. (37) into eq. (36), the following system of algebraic equations is obtained for the unknowns $\mathbf{x}_{\tau+\Delta\tau}$

$$\left[\frac{2}{\Delta\tau^2}\mathbf{L} + \mathbf{K}\right] x_{\tau+\Delta\tau} = \mathbf{L}\frac{1}{\Delta\tau^2}\left\{5\mathbf{x}_{\tau} - 4\mathbf{x}_{\tau-\Delta\tau} + \mathbf{x}_{\tau-2\Delta\tau}\right\} + \mathbf{P}. \tag{38}$$

To ensure the stability, the value of the time step has to be appropriately selected with respect to the material parameters (propagation velocities) and the time dependence of the boundary conditions.

4 Numerical examples

In order to test the accuracy of the present meshless method, a unit square panel under a sudden heating on the top side is analyzed as the first example (Fig. 2). Inertial effects are neglected here and the other boundary conditions are as indicated in the figure. The problem is, mathematically, one-dimensional and the following analytical solution is available for uncoupled thermoelasticity in a homogeneous isotropic material [Carslaw and Jaeger (1959), Timoshenko and Goodier (1951)]

$$\theta(x_2,\tau) = 1 - \frac{4}{\pi}\sum_{n=0}^{\infty}\frac{(-1)^n}{2n+1}\exp\left[-\frac{(2n+1)^2\pi^2\kappa\tau}{4a^2}\right]\cos\left(\frac{(2n+1)\pi x_2}{2a}\right),$$

$$u_2(x_2,\tau) = \frac{(1+\nu)\alpha}{(1-\nu)}\int_0^{x_2}\theta(x_2,\tau)dx_2,$$

$$\sigma_{11}(x_2,\tau) = -\frac{\alpha E}{(1-\nu)}\theta(x_2,\tau), \quad \sigma_{22}(x_2,\tau) = 0 \tag{39}$$

where a is the side length of the panel and $\kappa = k/\rho c$ is the diffusivity coefficient. In the numerical analysis here, the following material constants are used: $k = 2\cdot 10^5 \mathrm{m}^2/\mathrm{s}$, $\rho = 5000\mathrm{kgm}^{-3}$, $c = 3\cdot 10^6 \mathrm{Ws/kgdeg}$, $\alpha = 0.4\cdot 10^{-5}\,\mathrm{deg}^{-1}$, $E = 1\cdot 10^{11}\mathrm{Pa}$ and $\nu = 0.3$. Also, plane strain condition is assumed.

The mechanical displacement and the thermal fields on the finite square panel are approximated by using 441 (21x21) equi-spaced nodes. The local sub-domains are considered to be circular, each with a radius $r_{loc} = 0.035$. For the purpose of error

analysis the Sobolev-norm is calculated. The relative error of the temperature in the considered time interval $[0,T]$ is defined as

$$r = \frac{\|\theta^{num} - \theta^{exact}\|}{\|\theta^{exact}\|},$$

where $T = 10^5 s$ and

$$\|\theta\| = \left(\int_0^T \theta^2 d\tau \right)^{1/2}.$$

The relative error of the temperature r at both points (bottom and mid point) is less than 0.18% at the value of the time step $\Delta\tau = 250s$.

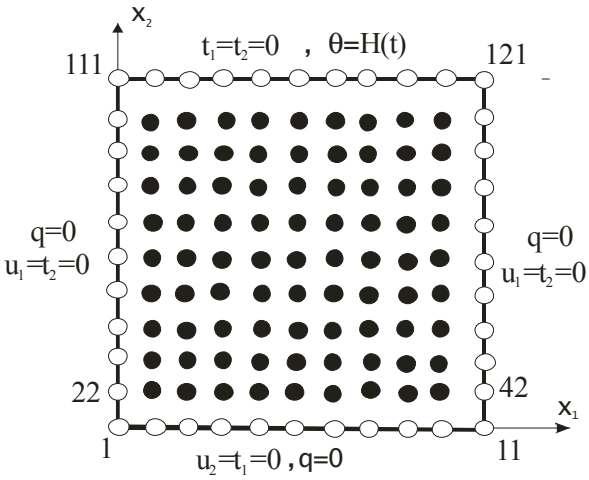

Figure 2: A suddenly heated unit square panel

The computed temporal variations of the temperature at the two different locations on the x_2- axis are shown in Fig. 3. Since FEM results will be used later for comparison when dealing with more complicated problems for which analytical solutions are not available, the accuracy of the FEM results obtained from the computer code ANSYS are also examined. The FEM results have been obtained using 1650 quadratic eight-noded elements and 1000 time steps. For the range of the time interval considered, it can be seen that there is quite good agreement of the temperature computed. Numerical results for the displacement u_2 at the free-end of the panel and at the mid-point of the x_2- axis are presented in Fig. 4. They are

compared again with the FEM results and excellent agreement is observed as well.

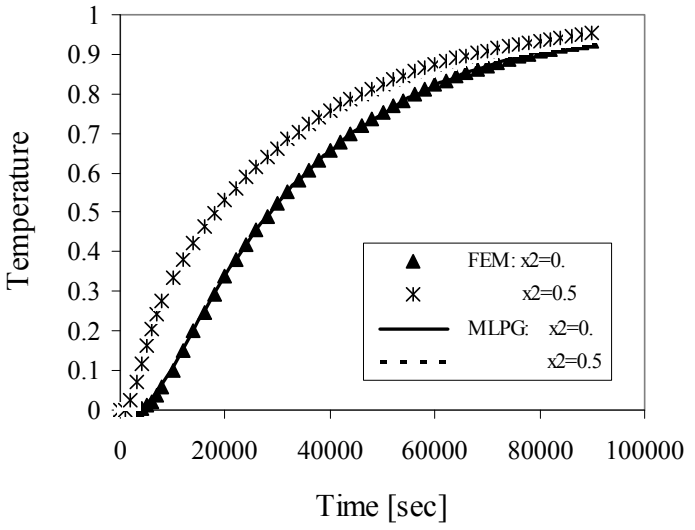

Figure 3: Temporal variation of the temperature at two different points on the x_2-axis

Next, functionally graded material properties in the x_2-direction are considered. An exponential variation of the elastic and thermal constants is assumed as

$$c_{ijkl}(\mathbf{x}) = c_{ijkl0}\exp(\gamma x_2), \quad k_{ij}(\mathbf{x}) = k_{ij0}\exp(-\gamma x_2), \tag{40}$$

where c_{ijkl0} and k_{ij0} correspond to the material parameters used in the previous example.

The magnitude of the elastic parameters increases with x_2-coordinate while the reverse is true for the heat conduction coefficients. This is quite typical of FGMs with increasing content of ceramic materials in the composition. The thermal expansion coefficient is taken to be uniform here, namely, with $\alpha = 0.4 \cdot 10^{-5}\,\mathrm{deg}^{-1}$. A value $\gamma = 0.5$ is assumed for the gradient parameter in the numerical calculations and the inertial mass effect is taken into account. The numerical results for the temporal variation of the temperature and the displacement u_2 at some locations are presented in Figs. 5 and 6, respectively. It can be seen that the stationary state in the FGM panel with a lower thermal conductivity is reached later than in a homo-

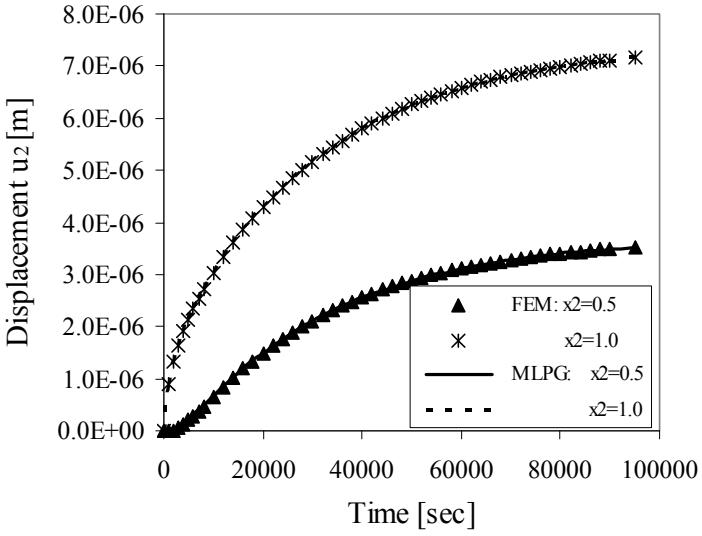

Figure 4: Temporal variation of the displacement u_2 at two different points on x_2-axis

geneous panel. Also, the displacements are slightly reduced in the FGM panel due to the higher elastic constants and the unchanged thermal expansion coefficient.

A transversely isotropic material with the following material constants is considered next: Young's moduli $E_1 = E_3 = 1 \cdot 10^{11} N/m^2$, $E_2 = 3 \cdot 10^{11} N/m^2$, Poisson's ratios $\nu_{12} = \nu_{32} = 0.1$, $\nu_{21} = \nu_{23} = \nu_{13} = 0.3$ and shear moduli $G_{12} = G_{23} = 38.46 \cdot 10^9 N/m^2$, $G_{13} = 115.4 \cdot 10^9 N/m^2$. The compliance matrix can be expressed in terms of the Young's moduli and Poisson's ratios

$$\beta_{11} = 1/E_1, \quad \beta_{22} = 1/E_2, \quad \beta_{33} = 1/E_3$$

$$\beta_{12} = \beta_{21} = -\nu_{12}/E_1 = -\nu_{21}/E_2, \quad \beta_{13} = \beta_{31} = -\nu_{13}/E_1 = -\nu_{31}/E_3$$

$$\beta_{23} = \beta_{32} = -\nu_{23}/E_2 = -\nu_{32}/E_3, \quad \beta_{44} = 1/G_{23},$$

$$\beta_{55} = 1/G_{13}, \quad \beta_{66} = 1/G_{12}.$$

The corresponding elastic stiffness matrix can be obtained by the inversion of the

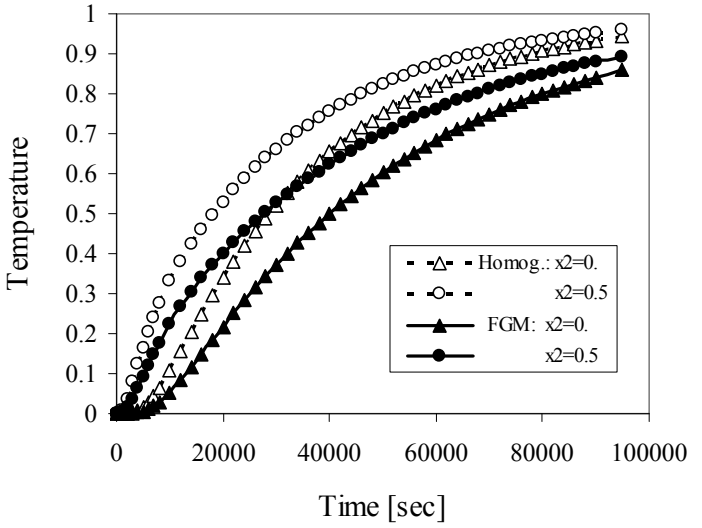

Figure 5: Comparison of the temporal variations of the temperature in homogeneous and FG materials

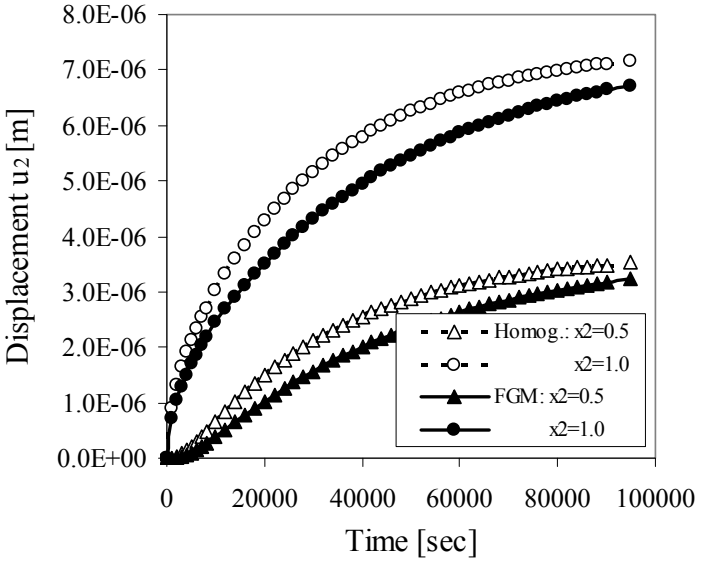

Figure 6: Comparison of the temporal variations of the displacement u_2 in homogeneous and FG materials

compliance matrix to be as follows:

$$\begin{bmatrix} 116.6 & 46.88 & 39.66 & 0 & 0 & 0 \\ & 328.1 & 46.88 & 0 & 0 & 0 \\ & & 116.6 & 0 & 0 & 0 \\ & & & 38.46 & 0 & 0 \\ & sym. & & & 115.4 & 0 \\ & & & & & 38.46 \end{bmatrix} \cdot 10^9 N/m^2.$$

The material considered here is evidently orthotropic in the $x_1 - x_2$ plane. The thermal conductivity coefficients are given as follows: $k_{11} = 2 \cdot 10^5 \mathrm{m}^2/\mathrm{s}$, $k_{22} = 1 \cdot 10^5 \mathrm{m}^2/\mathrm{s}$ and $k_{12} = 0$, and the thermal expansion coefficients are: $\alpha_{11} = \alpha_{33} = 0.4 \cdot 10^{-5}\,\mathrm{deg}^{-1}$ and$\alpha_{22} = 0.2 \cdot 10^{-5}\,\mathrm{deg}^{-1}$. For the purpose of comparison, the problem is also treated in isotropy, assuming the values of some of the following material properties of the above: $E = E_{11}$, $\nu = \nu_{12}, k = k_{11}$.

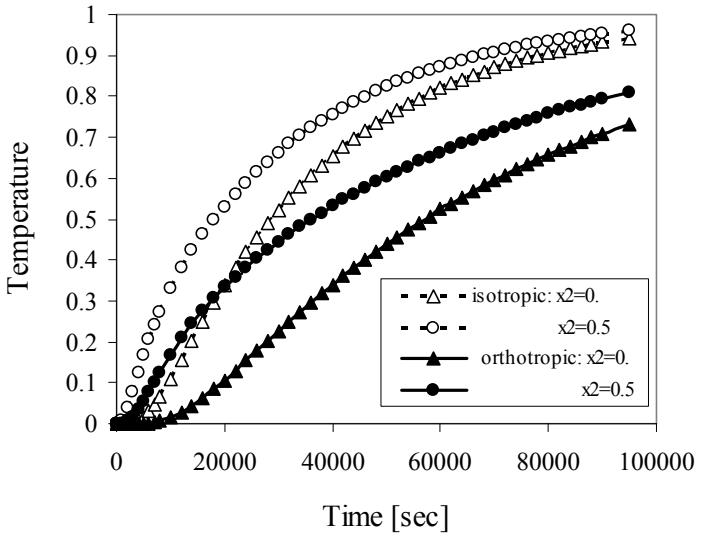

Figure 7: Comparison of the temporal variations of the temperature in isotropic and orthotropic homogeneous materials

The MLPG computed results for the time variations of the temperature and the displacements at x_2=0 and x_2=0.5 are given in Figs. 7 and 8, respectively. The thermal expansion coefficient for the orthotropic material in x_2-direction is smaller

than the isotropic material. However, Young's modulus in the same direction is 3 times higher than in the isotropic case. Then, the equivalent thermal forces in the orthotropic panel are only slightly higher than that in the isotropic panel. The displacement component u_2 is therefore significantly reduced in the orthotropic panel.

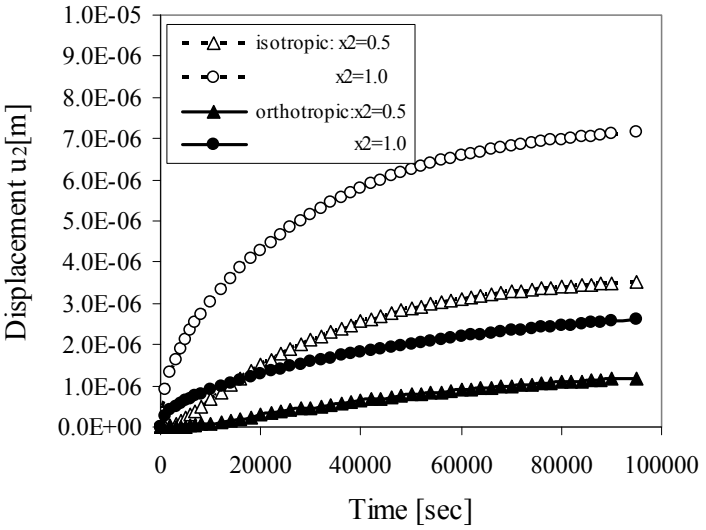

Figure 8: Comparison of the temporal variations of the displacement u_2 in isotropic and orthotropic homogeneous materials

The temporal variations of the stress σ_{11} at the mid-point for three different materials are given in Fig. 9; they are for the isotropic material, the orthotropic material and the FGM with exponential variation of the properties as per eq. (40) with $\gamma = 0.5$ as treated earlier. The elastic parameters at the mid-point of the panel are about 30% higher in the FGM panel than in the homogeneous counterpart. The stationary value of the stress for the FGM panel can thus be expected to be higher. Due to the reduced thermal conductivity in the FG panel with respect to the homogeneous case, the temperature in the FGM panel is lower at each time instant. For smaller time instants, the temperature reduction and the increase of elastic parameters at the mid of the FG panel are eliminated and the stress values for FGM and homogeneous materials are comparable. The stresses for the orthotropic panel are reduced compared to isotropic panel since the displacements are significantly reduced in the orthotropic panel.

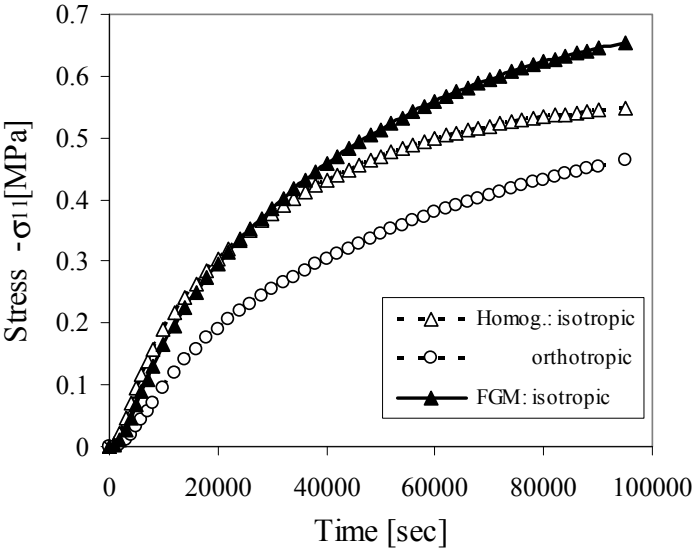

Figure 9: Temporal variation of the compressive stress σ_{11} at the mid-point

Next, an edge crack in a finite orthotropic strip is analyzed. Figure 10 shows one-half of the physical geometry that is modeled, advantage being taken of symmetry about the x_1-axis. The following values of the geometric parameters are considered: $a = 0.5$, $a/w = 0.4$ and $h/w = 1.2$. A total of 930 nodes equidistantly distributed for the MLS approximation of the physical quantities are employed. On the left lateral side of the strip a cooling thermal shock is applied. The material parameters are the same as those used in the previous examples.

For cracks in homogeneous, orthotropic, linear elastic solids, the asymptotic behaviour of the field quantities has been given by Sih et al. (1965). The asymptotic fields in the vicinity of the crack-tip in a continuously non-homogeneous medium are the same as in a homogeneous one [Eischen (1987]. For general mixed mode case, they may be expressed as follows:

$$\sigma_{11} = \frac{K_I}{\sqrt{2\pi r}} Re\left[\frac{\mu_1^{tip}\mu_2^{tip}}{\mu_1^{tip}-\mu_2^{tip}}\left(\frac{\mu_2^{tip}}{\sqrt{\cos\varphi+\mu_2^{tip}\sin\varphi}}-\frac{\mu_1^{tip}}{\sqrt{\cos\varphi+\mu_1^{tip}\sin\varphi}}\right)\right]$$

$$+\frac{K_{II}}{\sqrt{2\pi r}} Re\left[\frac{1}{\mu_1^{tip}-\mu_2^{tip}}\left(\frac{(\mu_2^{tip})^2}{\sqrt{\cos\varphi+\mu_2^{tip}\sin\varphi}}-\frac{(\mu_1^{tip})^2}{\sqrt{\cos\varphi+\mu_1^{tip}\sin\varphi}}\right)\right],$$

$$\sigma_{22} = \frac{K_I}{\sqrt{2\pi r}} Re\left[\frac{1}{\mu_1^{tip}-\mu_2^{tip}}\left(\frac{\mu_1^{tip}}{\sqrt{\cos\varphi+\mu_2^{tip}\sin\varphi}}-\frac{\mu_2^{tip}}{\sqrt{\cos\varphi+\mu_1^{tip}\sin\varphi}}\right)\right]$$

$$+\frac{K_{II}}{\sqrt{2\pi r}} Re\left[\frac{1}{\mu_1^{tip}-\mu_2^{tip}}\left(\frac{1}{\sqrt{\cos\varphi+\mu_2^{tip}\sin\varphi}}-\frac{1}{\sqrt{\cos\varphi+\mu_1^{tip}\sin\varphi}}\right)\right],$$

$$\sigma_{12} = \frac{K_I}{\sqrt{2\pi r}} Re\left[\frac{\mu_1^{tip}\mu_2^{tip}}{\mu_1^{tip}-\mu_2^{tip}}\left(\frac{1}{\sqrt{\cos\varphi+\mu_1^{tip}\sin\varphi}}-\frac{1}{\sqrt{\cos\varphi+\mu_2^{tip}\sin\varphi}}\right)\right]$$

$$+\frac{K_{II}}{\sqrt{2\pi r}} Re\left[\frac{1}{\mu_1^{tip}-\mu_2^{tip}}\left(\frac{\mu_1^{tip}}{\sqrt{\cos\varphi+\mu_1^{tip}\sin\varphi}}-\frac{\mu_2^{tip}}{\sqrt{\cos\varphi+\mu_2^{tip}\sin\varphi}}\right)\right],$$

$$u_1 = K_I\sqrt{\frac{2r}{\pi}}$$

$$Re\left[\frac{1}{\mu_1^{tip}-\mu_2^{tip}}\left(\mu_1^{tip}P_{12}\sqrt{\cos\varphi+\mu_2^{tip}\sin\varphi}-\mu_2^{tip}P_{11}\sqrt{\cos\varphi+\mu_1^{tip}\sin\varphi}\right)\right]$$

$$+K_{II}\sqrt{\frac{2r}{\pi}} Re\left[\frac{1}{\mu_1^{tip}-\mu_2^{tip}}\left(P_{12}\sqrt{\cos\varphi+\mu_2^{tip}\sin\varphi}-P_{11}\sqrt{\cos\varphi+\mu_1^{tip}\sin\varphi}\right)\right],$$

$$u_2 = K_I\sqrt{\frac{2r}{\pi}}$$

$$Re\left[\frac{1}{\mu_1^{tip}-\mu_2^{tip}}\left(\mu_1^{tip}P_{22}\sqrt{\cos\varphi+\mu_2^{tip}\sin\varphi}-\mu_2^{tip}P_{21}\sqrt{\cos\varphi+\mu_1^{tip}\sin\varphi}\right)\right]$$

$$+K_{II}\sqrt{\frac{2r}{\pi}} Re\left[\frac{1}{\mu_1^{tip}-\mu_2^{tip}}\left(P_{22}\sqrt{\cos\varphi+\mu_2^{tip}\sin\varphi}-P_{21}\sqrt{\cos\varphi+\mu_1^{tip}\sin\varphi}\right)\right], \tag{41}$$

where (r,φ) are polar coordinates with the origin at the crack-tip and related to the local Cartesian coordinate system (x_1,x_2). Also, in eq. (41), Re denotes the real part of a complex function, μ_i^{tip} are material parameters at the crack-tip, which are roots of the following characteristic equation in terms of the elastic compliances β_{mn} (m,n = 1, 2 and 6) of the anisotropic material (Lekhnitskii, 1963)

$$\beta_{11}\mu^4 - 2\beta_{16}\mu^3 + (2\beta_{12}+\beta_{66})\mu^2 - 2\beta_{26}\mu + \beta_{22} = 0. \tag{42}$$

The stress intensity factors (SIFs) K_I and K_{II} can be computed by the extrapolation technique if the auxiliary quantities $K_{I,II}(\delta)$ are computed at several points on the crack-surface at distances δ from the crack-tip. In a pure mode-I these quantities are computed from

$$K_I(\delta) = \frac{u_2(\delta)}{D_{21}} \sqrt{\frac{\pi}{2\delta}}, \tag{43}$$

where

$$D_{21} = Re \left\{ \frac{\mu_1^{tip} P_{22} - \mu_2^{tip} P_{21}}{\mu_1^{tip} - \mu_2^{tip}} \right\} \tag{44}$$

and

$$P_{ik} = \begin{bmatrix} \beta_{11}\mu_k^2 + \beta_{12} - \beta_{16}\mu_k \\ \beta_{12}\mu_k + \beta_{22}/\mu_k - \beta_{26} \end{bmatrix}. \tag{45}$$

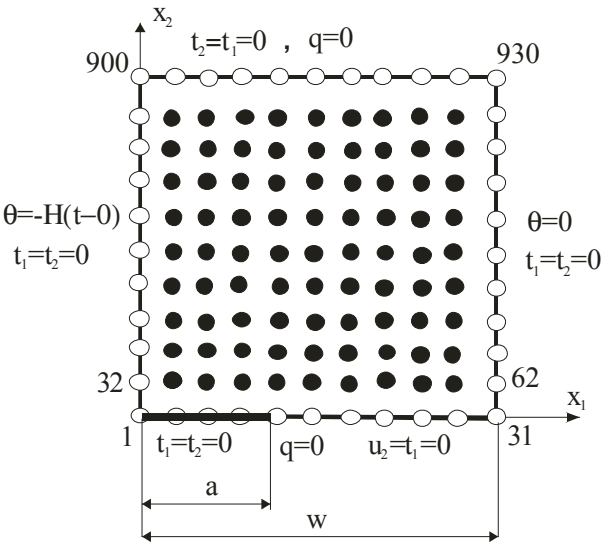

Figure 10: Numerical model of the problem of an edge crack in a finite strip under a thermal shock on the lateral side

For this crack problem, isotropic material properties are first considered. The time variation of the normalized stress intensity factor $f_I = K_I/\alpha_{11}c_{11}\theta_0\sqrt{\pi a}$ is given in

Fig. 11. There is clearly good agreement of the present MLPG and the ANSYS-FEM results; the latter have been obtained with 2812 quadratic (8-node) elements. The stress intensity factor vanishes for large time instants due to vanishing stresses ahead of the crack-tip in a stationary state.

With the same geometry and boundary conditions as considered in the previous case, the material properties are next taken to be orthotropic with the same elastic constants used earlier. The heat conduction coefficient for the orthotropic material in the x_1-direction is the same as in the isotropic case. Since the heat flux caused by a thermal gradient is only in the x_1-direction, the orthotropic thermal properties have no influence on the temperature distribution. Thus, one can observe in Fig. 12, peak values of the SIF at the same instant for both the isotropic and orthotropic materials. The thermal forces for the orthotropic material are higher due to the higher increase of Young's modulus in x_2-direction than the decrease of the thermal expansion coefficient. Therefore, the peak value of SIF is higher for the orthotropic material than for the isotropic one.

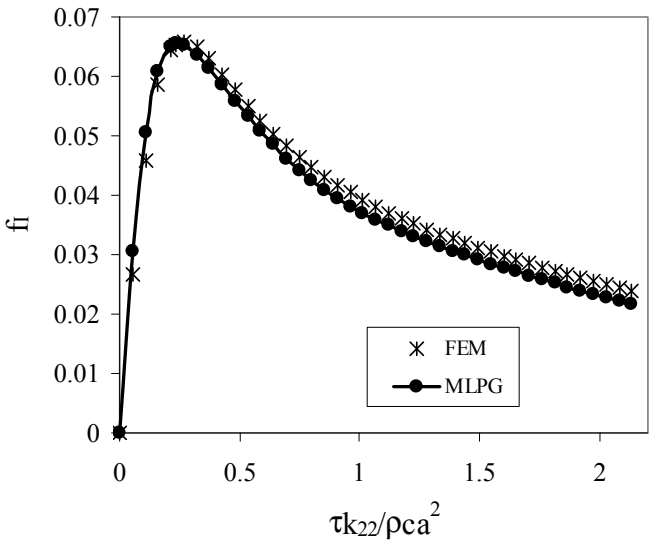

Figure 11: Temporal variation of the normalized SIF for isotropic case

For the last example, 3-D analysis of a clamped L-shaped console is presented. The geometry and boundary conditions are as shown on Fig. 13. It is the same problem as that which have been treated by Kögl and Gaul (2003) using the dual reciprocity BEM, thus allowing comparison of the present results with those obtained by them

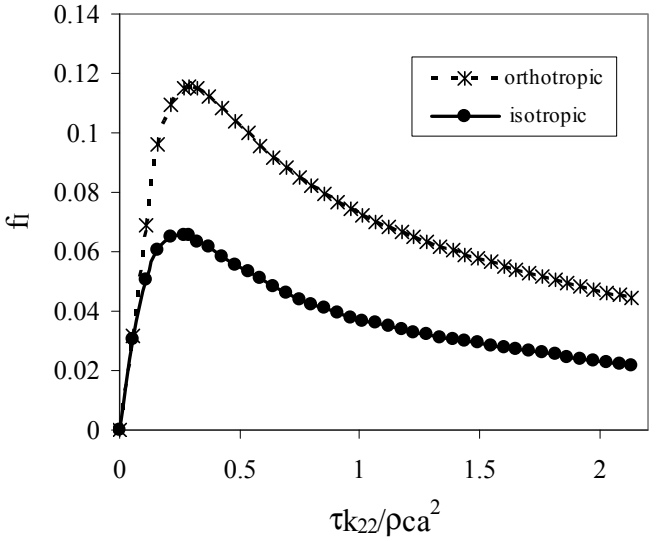

Figure 12: Comparison of the temporal variations of the SIFs in isotropic and orthotropic strips

to be made. The following parameters for a monoclinic material are used:
For the stiffness matrix,

$$\mathbf{C} = \begin{bmatrix} 430.1 & 130.4 & 18.2 & 0 & 0 & 201.3 \\ 130.4 & 116.7 & 21 & 0 & 0 & 70.1 \\ 18.2 & 21 & 73.6 & 0 & 0 & 2.4 \\ 0 & 0 & 0 & 19.8 & -8 & 0 \\ 0 & 0 & 0 & -8 & 29.1 & 0 \\ 201.3 & 70.1 & 2.4 & 0 & 0 & 147.3 \end{bmatrix} GPa;$$

the stress-temperature coefficients

$$\boldsymbol{\gamma} = \begin{bmatrix} 1.01 & 2 & 0 \\ 2 & 1.48 & 0 \\ 0 & 0 & 7.52 \end{bmatrix} * 10^6 N/\deg m^2;$$

the thermal conductivity constants

$$\mathbf{k} = \begin{bmatrix} 5.2 & 0 & 0 \\ 0 & 7.6 & 0 \\ 0 & 0 & 38.3 \end{bmatrix} W/\deg m;$$

the mass density $\rho = 7820kg/m^3$, and the heat capacity $c = 461J/\deg kg$.

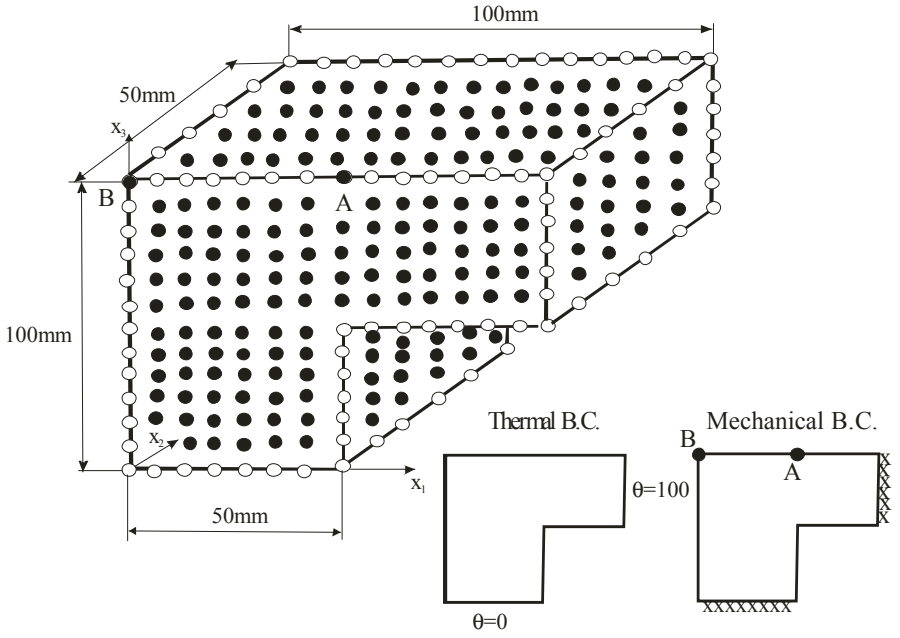

Figure 13: Clamped L-shaped console under a thermal load

A distribution of equi-spaced nodes in the $x_1 - x_3$ plane is used with a distance of 5mm between two neighbouring nodes; there are 341 nodes in each cross section. The distance between two neighbouring cross sections in the x_2-axis is 10mm. The total number of nodes is thus 6*341=2046. Stationary boundary conditions are considered first here. The computed variations of the temperature along the x_3-axis at $x_1 = 50mm$ and $x_2 = 0$ are shown in Fig. 14. There is good agreement of the results obtained by the present MLPG and the dual reciprocity BEM.. The variation of the displacement component u_3 along the same line is given in Fig. 15 where again good agreement of the two sets of results is observed.

Finally, transient thermal conditions with Heaviside time variation of a prescribed temperature on the right lateral clamped side is considered for the three dimensional problem. All the other boundary conditions and material parameters are the same as in the stationary case treated above. The time variations of temperature and displacements at the nodes A and B as indicated in Fig. 13 are shown in Figs. 16 and 17, respectively; the temporal axis is normalized, where $a = 0.01m$ is the maximum dimension of the L-shaped console. Numerical results of the displacements

at node A are normalized by the static quantity $u_3^{stat} = 0.102mm$ and compared with FEM results. It can be seen that there are some minimal discrepancies only when the instants are small.

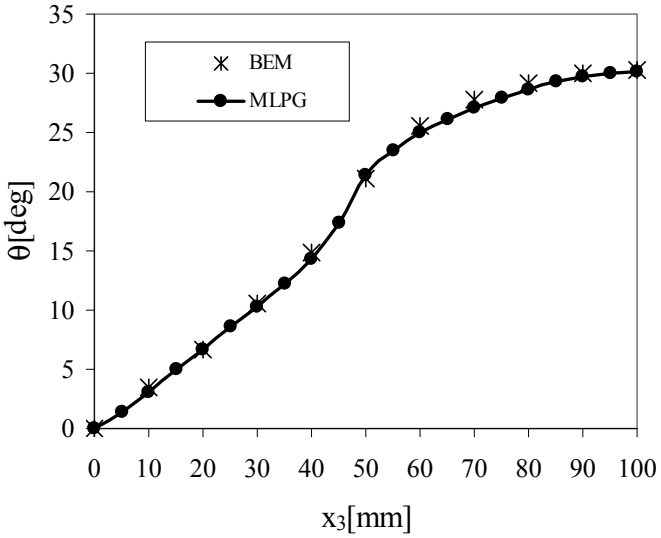

Figure 14: Variation of the temperature along x_3.-axis at $x_1 = 50mm$ under stationary conditions

5 Conclusions

A meshless local Petrov-Galerkin method (MLPG) is presented for two- and three-dimensional transient thermoelasticity of orthotropic, linear elastic solids, the material properties of which can be continuously varying in space. The backward finite-difference method is applied for the approximation of the diffusive term in the heat conduction equation. The mechanical fields are described by the equations of motion with the inertial term. In the numerical analysis, the solution domain is divided into small overlapping circular (2-D) or spherical (3-D) subdomains. A unit step function is used as the test functions in the local weak-form. The moving least-squares (MLS) scheme is adopted for approximating the physical quantities. After performing the spatial integrations, one obtains a system of ordinary differential equations for certain nodal unknowns. That system is solved numerically by the Houbolt finite-difference time-stepping scheme. The proposed method is a truly meshless method which requires neither domain elements nor background cells in

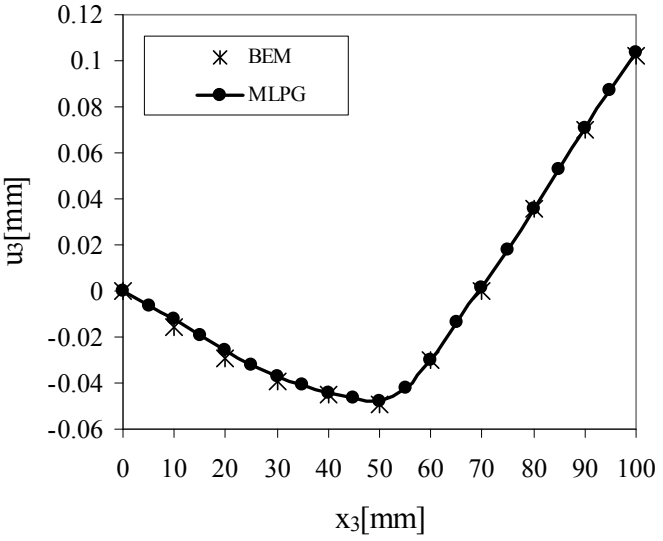

Figure 15: Variation of the displacement u_3 along x_3-axis at $x_1 = 50mm$ under stationary conditions

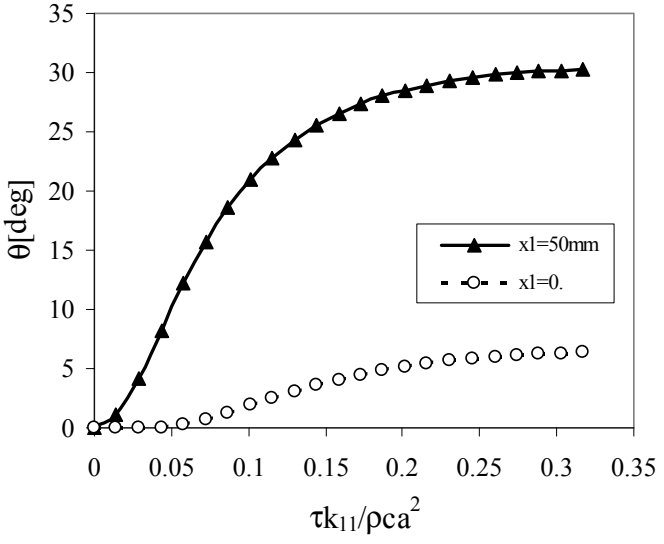

Figure 16: Time variation of the temperature at nodes A and B

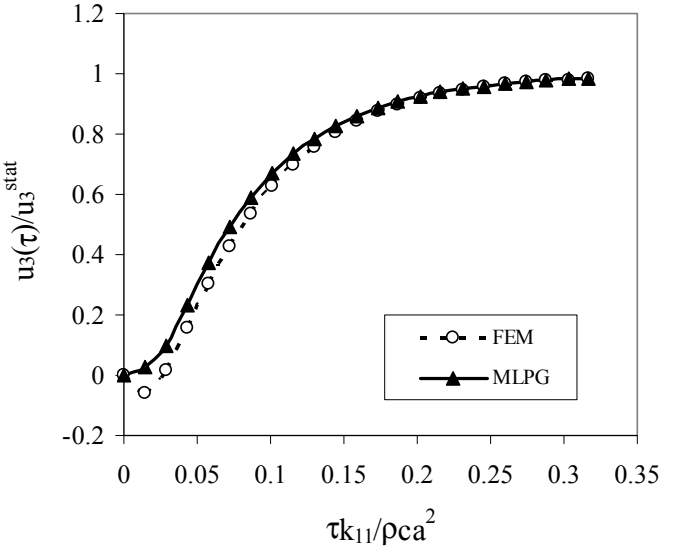

Figure 17: Time variation of the displacements at node A

either the interpolation or the integration. It has been illustrated by a number of examples where good agreement of the results obtained by this MLPG method and other available solutions has been demonstrated.

The present method is an alternative numerical tool to many existing computational methods. Its main advantage is its applicability for general boundary value problems. The conventional BEM is a very power computational method if the fundamental solution is available and has simple mathematical forms. In many cases, however, such as for general FGMs, the fundamental solution is either not available, or is very complicated which can significantly affect its efficiency. The present method requires no fundamental solutions; the test function is simple and all integrands in the present formulation are regular thereby requiring no special numerical techniques for the evaluation of the integrals. The present formulation possesses the generality of the FEM. It therefore offers great promise for numerical analysis of multi-field problems which cannot be solved efficiently by, e.g., the conventional BEM. Moreover, the present meshless method is evidently more flexible than the standard FEM, since an adaptation of the nodal distribution is easier than an element-based mesh adaptation.

Acknowledgement: The authors acknowledge the support by the Slovak Sci-

ence and Technology Assistance Agency registered under number APVV-0427-07, the Slovak Grant Agency VEGA-2/0039/09, and the German Research Foundation (DFG, ZH 15/10-1).

References

Anlas, G.; Santare, M.H.; Lambros, J. (2000): Numerical calculation of stress intensity factors in functionally graded materials. *Int. J. Fracture*, 104: 131-143.

Atluri, S.N. (2004): *The Meshless Method, (MLPG) For Domain & BIE Discretizations*, Tech Science Press.

Atluri, S.N.; Zhu, T. (1998): A New Meshless Local Petrov-Galerkin (MLPG) Approach in Computational Mechanics. *Computational Mechanics*, 22: 117-127.

Atluri, S.N.; Sladek, J.; Sladek, V.; Zhu, T. (2000): The local boundary integral equation (LBIE) and its meshless implementation for linear elasticity. *Comput. Mech.*, 25: 180-198.

Atluri, S.N.; Han, Z.D.; Shen, S.P. (2003): Meshless local Petrov-Galerkin (MLPG) approaches for solving the weakly-singular traction & displacement boundary integral equations. *CMES: Computer Modeling in Engineering & Sciences*, 4: 507-516.

Atluri, S.N.; Shen, S.P. (2002): The meshless local Petrov-Galerkin (MLPG) method: A simple & less costly alternative to the finite element and boundary element methods. *CMES: Computer Modeling in Engineering & Sciences*, 3: 11-51.

Atluri, S.N.; Shen, S.P. (2002): *The Meshless Local Petrov-Galerkin (MLPG) Method*, 440 pages, Tech Science Press.

Batra, R.C.; Porfiri, M.; Spinello, D. (2004): Treatment of material discontinuity in two Meshless local Petrov-Galerkin (MLPG) formulations of axisymmetric transient heat conduction. *Int. J. Num. Meth. Engn.*, 61: 2461-2479.

Belytschko, T.; Krogauz, Y.; Organ, D.; Fleming, M.; Krysl, P. (1996): Meshless methods; an overview and recent developments. *Comp. Meth. Appl. Mech. Engn.*, 139: 3-47.

Bobaru, F.; Mukherjee, S. (2003): Meshless approach to shape optimization of linear thermoelastic solids. *Int. J. Num. Meth. Engn.*, 53: 765-796.

Carslaw, H.S.; Jaeger, J.C. (1959): *Conduction of Heat in Solids*, Clarendon, Oxford.

Chen, J.; Dargush, G.F. (1995): Boundary element method for dynamic poroelastic and thermoelastic analyses. *Int. J. Solids and Structures*, 32: 2257-2278.

Chan, Y.; Gray, L.J.; Kaplan, T.; Paulino, G.H. (2004): Green's function for a

two-dimensional exponentially graded elastic medium. *Proceedings Royal Society London* A, 460: 1689-1706.

Ching, H.K.; Chen, J.K. (2006): Thermomechanical analysis of functionally graded composites under laser heating by the MLPG method. *CMES: Computer Modeling in Engineering & Sciences*, 13 (3): 199-217.

Criado, R.; Ortiz, J.E.; Mantic, V.; Gray, L.J.; Paris, F. (2008): Green's function for three dimensional exponentially graded elasticity. *International Journal for Numerical Methods in Engineering*, 74: 1560-1591.

Dargush, G.F.; Banerjee, P.K. (1991): A new boundary element method for three-dimensional coupled problems of conduction and thermoelasticity. *ASME J. Appl. Mech.*, 58: 28-36.

Eischen, J.W. (1987): Fracture of nonhomogeneous materials. *International Journal of Fracture*, 34: 3-22.

Erdogan F., Wu B.H. (1996) Crack problems in FGM layers under thermal stresses. *J. Thermal Stresses*, 19: 237-265.

Eshelby, J.D; Read, W.T.; Shockley, W. (1953): Anisotropic elasticity with applications to dislocations. *Acta Metallurgica*, 1: 251-259.

Fleming, M.; Chu, Y.A.; Moran, B.; Belytschko, T. (1997): Enriched element-free Galerkin methods for crack tip fields. *International Journal for Numerical Methods in Engineering*, 40: 1483-1504.

Gaul, L.; Kögl, M.; Wagner, M. (2003): *Boundary Element Methods for Engineers and Scientists*. Springer-Verlag, Berlin.

Han, Z.D.; Atluri, S.N. (2004a): Meshless local Petrov-Galerkin (MLPG) approaches for solving 3D problems in elasto-statics. *CMES: Computer Modeling in Engineering & Sciences*, 6: 169-188.

Han, Z.D.; Atluri, S.N. (2004b): A meshless local Petrov-Galerkin (MLPG) approach for 3-dimensional elasto-dynamics. *CMC: Computers, Materials & Continua*, 1: 129-140.

Hosseini-Tehrani, P.; Eslami, M.R. (2000): BEM analysis of thermal and mechanical shock in a two-dimensional finite domain considering coupled thermoelasticity. *Engineering Analysis with Boundary Elements*, 24: 249-257.

Jin Z.H. (2002): An asymptotic solution of temperature field in a strip of a functionally graded material. *Int. Comm. Heat Mass Transfer*, 29: 887-895.

Jin Z.H.; Noda N. (1993): An internal crack parallel to the boundary of a nonhomogeneous half plane under thermal loading. *Int. J. Eng. Sci.,* 31: 793-806.

Jin Z.H.; Batra R.C. (1996): Stress intensity relaxation at the tip of an edge crack

in a functionally graded material subjected to a thermal shock. *J. Thermal Stresses,* 19: 317-339

Jin Z.H.; Paulino G.H. (2001): Transient thermal stress analysis of an edge crack in a functionally graded material. *Int. J. Fract*. 107: 73-98

Kim J.H.; Paulino G.H. (2002): Isoparametric graded finite elements for nonhomogeneous isotropic and orthotropic materials. *J. Appl. Mech*. 69: 502-514.

Keppas, L.K.; Giannopoulos, G.I.; Anifantis, N.K. (2008): Transient coupled thermoelastic contact problems incorporating thermal resistance: a BEM approach. *CMES: Computer Modeling in Engineering & Sciences*, 25: 181-196.

Kögl, M.; Gaul, L. (2003): A boundary element method for anisotropic coupled thermoelasticity. *Arch. Appl. Mech*., 73: 377-398.

Lekhnitskii, S.G. (1963): *Theory of Elasticity of an Anisotropic Body*, Holden Day, San Francisco.

Martin, P.A.; Richardson, J.D.; Gray, L.J.; Berger, J.R. (2002): On Green's function for a three-dimensional exponentially graded elastic solid. *Proceedings of Royal Society London* A, 458: 1931-1947.

Miyamoto, Y.; Kaysser, W.A.; Rabin, B.H.; Kawasaki, A.; Ford, R.G. (1999): *Functionally Graded Materials; Design, Processing and Applications*, Kluwer Academic Publishers, Dordrecht.

Noda N.; Jin Z.H. (1993) Thermal stress intensity factors for a crack in a strip of a functionally gradient material. *Int. J. Solids and Struct*., 30: 1039-1056.

Noda N.; Jin Z.H. (1994) A crack in functionally gradient materials under thermal shock. *Arch. Appl. Mech.,* 64: 99-110.

Nowacki, W. (1986): *Thermoelasticity*, Pergamon, Oxford.

Park, K.H.; Banerjee, P.K. (2002): Two- and three-dimensional transient thermoelastic analysis by BEM via particular integrals. *Int. J. Solids and Structures*, 39: 2871-2892.

Qian, L.F.; Batra, R.C. (2004): Transient thermoelastic deformations of thick functionally graded plate. *Jour. Thermal Stresses*, 27: 705-740.

Santare, M.H.; Lambros, J. (2000): Use of graded finite elements to model the behavior of nonhomogeneous materials, *Journal of Applied Mechanics*, 67: 819-822.

Sellountos, E.J.; Polyzos, D. (2003): A MLPG (LBIE) method for solving frequency domain elastic problems. *CMES: Computer Modeling in Engineering & Sciences*, 4: 619-636.

Sellountos, E.J.; Vavourakis, V.; Polyzos, D. (2005): A new singular/hypersingular

MLPG (LBIE) method for 2D elastostatics. *CMES: Computer Modeling in Engineering & Sciences*, 7: 35-48.

Sellountos, E.J.; Sequeira, A.; Polyzos, D. (2009): Elastic transient analysis with MLPG (LBIE) method and local RBF's. *CMES: Computer Modeling in Engineering & Sciences*, 41: 215-241.

Schclar, S.N. (1994): *Anisotropic Analysis Using Boundary Elements*, Computational Mechanics Publications.

Shiah, Y.C.; Tan, C.L. (1999): Exact boundary integral transformation of the thermoelastic domain integral in BEM for general 2D anisotropic elasticity. *Computational Mechanics*, 23: 87-96.

Shiah, Y.C.; Tan, C.L.; Lee, V.G. (2008): Evaluation of explicit-form fundamental solutions for displacements and stresses in 3D anisotropic elastic solids. *CMES: Computer Modeling in Engineering & Sciences*, 34: 205-226.

Sih, G.C.; Paris, P.C. and Irwin, G.R. (1965): On cracks in rectilinearly anisotropic bodies. *Int. J. Fracture Mechanics*, 1: 189-203

Sladek, V.; Sladek, J. (1984): Boundary integral equation method in thermoelasticity. Part I: General analysis. *Appl. Math. Modelling*, 7: 241-253.

Sladek, J.; Sladek, V.; Atluri, S.N. (2001): A pure contour formulation for meshless local boundary integral equation method in thermoelasticity. *CMES: Computer Modeling in Engn. & Sciences*, 2: 423-434.

Sladek, J.; Sladek, V.; Zhang, Ch. (2003a): Transient heat conduction analysis in functionally graded materials by the meshless local boundary integral equation method. *Computational Mechanics of Materials*, 28: 494-504.

Sladek, J.; Sladek, V.; Krivacek, J.; Zhang, Ch. (2003b): Local BIEM for transient heat conduction analysis in 3-D axisymmetric functionally graded solids. *Computational Mechanics*, 32: 169-176.

Sladek, J.; Sladek, V.; Atluri, S.N. (2004a): Meshless local Petrov-Galerkin method for heat conduction problem in an anisotropic medium. *CMES: Computer Modeling in Engineering & Sciences*, 6: 309-318.

Sladek, J.; Sladek, V.; Atluri, S.N. (2004b): Meshless local Petrov-Galerkin method in anisotropic elasticity. *CMES: Computer Modeling in Engn. & Sciences*, 6: 477-489.

Sladek, V.; Sladek, J.; Tanaka, M.; Zhang, Ch. (2005a): Transient heat conduction in anisotropic and functionally graded media by local integral equations. *Engineering Analysis with Boundary Elements,* 29: 1047-1065.

Sladek, J.; Sladek, V.; Krivacek, J.; Zhang, Ch. (2005b): Meshless Local Petrov-Galerkin Method for stress and crack analysis in 3-D axisymmteric FGM

bodies, *CMES: Computer Modeling in Engineering & Sciences,* 8: 259-270.

Sladek, J.; Sladek, V.; Zhang, Ch.; Tan C.L. (2006): Meshless local Petrov-Galerkin Method for linear coupled thermoelastic analysis, *CMES: Computer Modeling in Engineering & Sciences,* 16: 57-68.

Sladek, J.; Sladek, V.; Hellmich, Ch.; Eberhardsteiner, J. (2007a): Heat conduction analysis of 3D axisymmetric and anisotropic FGM bodies by meshless local Petrov-Galerkin method. *Computational Mechanics,* 39: 2007, 323-333.

Sladek, J.; Sladek, V.; Zhang, Ch.; Solek, P.; Starek, L. (2007b): Fracture analyses in continuously nonhomogeneous piezoelectric solids by the MLPG, *CMES: Computer Modeling in Engineering & Sciences*, 19: 247-262.

Sladek, J.; Sladek, V.; Solek, P.; Wen, P.H. (2008a): Thermal bending of Reissner-Mindlin plates by the MLPG, *CMES: Computer Modeling in Engineering & Sciences* 28: 57-76.

Sladek, J.; Sladek, V.; Solek, P.; Wen, P.H.; Atluri, S.N. (2008b): Thermal analysis of Reissner-Mindlin shallow shells with FGM properties by the MLPG, *CMES: Computer Modeling in Engineering & Sciences* 30: 77-97.

Sladek, J.; Sladek, V.; Tan C.L.; Atluri, S.N. (2008c): Analysis of transient heat conduction in 3D anisotropic functionally graded solids by the MLPG, *CMES: Computer Modeling in Engineering & Sciences* 32: 161-174.

Sladek, V.; Sladek, J.; Zhang, Ch. (2008d): Computation of stresses in non-homogeneous elastic solids by local integral equation method: a comparative study. *Computational Mechanics* 41: 827-845.

Sladek, V.; Sladek, J.; Zhang, Ch. (2008e): Local integral equation formulation for axially symmetric problems involving elastic FGM. *Engineering Analysis with Boundary Elements* 32: 1012-1024.

Sladek, J.; Sladek, V.; Solek, P. (2009): Elastic analyses in 3D anisotropic functionally graded solids by the MLPG. *CMES: Computer Modeling in Engineering & Sciences* 43: 223-251.

Suh, I.G.; Tosaka, N. (1989): Application of the boundary element method to 3-D linear coupled thermoelasticity problems. *Theor. Appl. Mech.*, 38: 169-175.

Suresh, S.; Mortensen A. (1998): *Fundamentals of Functionally Graded Materials.* Institute of Materials, London.

Sutradhar, A.; Paulino, G.H.; Gray, L.J. (2002): Transient heat conduction in homogeneous and non-homogeneous materials by the Laplace transform Galerkin boundary element method. *Engn. Analysis with Boundary Elements*, 26: 119-132.

Timoshenko, S.P.; Goodier, J.N. (1951): *Theory of Elasticity*, McGraw-Hill, New York.

Wang, H.; Qin, Q.H.; Kang, Y.L. (2006): A meshless model for transient heat conduction in functionally graded materials. *Computational Mechanics*, 38: 51-60.

Zhu, T.; Zhang, J.D.; Atluri, S.N. (1998): A local boundary integral equation (LBIE) method in computational mechanics, and a meshless discretization approaches. *Computational Mechanics,* 21: 223-235.